



Warm ocean anomaly, air sea fluxes, and the rapid intensification of tropical cyclone Nargis (2008)

I.-I. Lin,¹ Chi-Hong Chen,¹ Iam-Fei Pun,¹ W. Timothy Liu,² and Chun-Chieh Wu¹

Received 26 August 2008; revised 27 October 2008; accepted 7 November 2008; published 11 February 2009.

[1] On 2 May 2008, category-4 tropical cyclone Nargis devastated Myanmar. It was observed that just prior to its landfall, Nargis rapidly intensified from a weak category-1 storm to an intense category-4 storm within only 24 h. Using in situ ocean depth-temperature measurements and satellite altimetry, it is found that Nargis' rapid intensification took place on a pre-existing warm ocean anomaly in the Bay of Bengal. In the anomaly, the subsurface ocean is evidently warmer than climatology, as characterized by the depth of the 26°C isotherm of 73–101 m and the tropical cyclone heat potential of 77–105 kJ cm⁻². This pre-existing deep, warm subsurface layer leads to reduction in the cyclone-induced ocean cooling, as shown from the ocean mixed layer numerical experiments. As a result, there was a near 300% increase in the air-sea enthalpy flux to support Nargis' rapid intensification. **Citation:** Lin, I.-I., C.-H. Chen, I.-F. Pun, W. T. Liu, and C.-C. Wu (2009), Warm ocean anomaly, air sea fluxes, and the rapid intensification of tropical cyclone Nargis (2008), *Geophys. Res. Lett.*, 36, L03817, doi:10.1029/2008GL035815.

1. Introduction

[2] In May 2008, intense category-4 (in Saffir-Simpson tropical cyclone scale) Tropical Cyclone Nargis (2008) devastated Myanmar. The death toll exceeded 130,000 together with tremendous other losses; the estimated size of severely-affected population reached 1.5 million [Webster, 2008]. Improvement in understanding of such catastrophic event is imperative to control and reduce losses of this magnitude in the future. One critical issue that needs to be addressed is on Nargis' rapid (or sudden) intensification (RI, usually defined as ≥ 30 kts intensification in 24 h [Kaplan and DeMaria, 2003]) [DeMaria et al., 2005; Ventham and Wang, 2007]. It has been observed that just prior to hitting landfall, Nargis intensified rapidly from a weak category-1 storm to an intense category-4 storm in a day. This threat coupled with the communication difficulties [Webster, 2008] expose the large, vulnerable population living along the Myanmar's coasts great danger. As ocean is the energy source for intensification [Emanuel, 1999; Shay et al., 2000; Lin et al., 2005, 2008; Wu et al., 2007; I.-I. Lin et al., Upper ocean thermal structure and the western North Pacific category-5 typhoons—Part II: Dependence on translation speed, submitted to *Monthly Weather Review*, 2008], in this work we investigate the role of upper ocean thermal structure (UOTS,

typically from surface down to the 100–200 m depth) and the associated air-sea interaction processes played in Nargis' RI. Especially, there is limited prior study on this subject for the Northern Indian Ocean/Bay of Bengal cyclones [Ali et al., 2007].

[3] In Section 2, observational results are presented. In situ depth-temperature profiles from the Argo floats [Gould et al., 2004] and the NOAA/GTSPP (Global Temperature and Salinity Profile Program) data base are searched to depict the detail UOTS structure. Sea surface height anomaly (SSHA) map from the JASON-1, ENVISAT, and GFO (GEOSAT Follow-On) satellite altimeters (data source: near real time product from the Ssalto/Duacs and distributed by Aviso) are used to observe the synoptic situation on ocean features [Shay et al., 2000; Goni and Trinanes, 2003; Lin et al., 2005, 2008; Ali et al., 2007]. Also, the observed SSHA data is used in a 2-layer reduced gravity ocean model [Shay et al., 2000; Goni and Trinanes, 2003; Pun et al., 2007] to derive UOTS in regions where no suitable in situ profiles are available. The cyclone track and intensity data is from the Unisys Weather (<http://weather.unisys.com/hurricane/>). In Section 3, numerical experiments using the Price-Weller-Pinkel [Price et al., 1986] ocean mixed layer model are conducted to study the air-sea interaction during the RI period. The drag coefficient (C_d) used is based on Powell et al. [2003]. Air-sea enthalpy fluxes are subsequently estimated using the bulk aerodynamic formulae [Black et al., 2007; Lin et al., 2008, also submitted manuscript, 2008]. Discussion and conclusion are presented in Section 4.

2. Observations

[4] Figure 1a depicts the SSHA condition observed just prior to Nargis' RI. It can be seen that the RI process (from 1800 UTC 30 April–0600 UTC 2 May 2008, Figure 1b) took place pre-dominantly over warm ocean anomaly regions characterized by positive SSHA between 6–20 cm. Within the 24 h between 0600 UTC 1 May–0600 UTC 2 May, it intensified from category-1 (75 kts) to its peak at category-4 (115 kts) (Figure 1b). It is also observed that around 0000 UTC 2 May, Nargis passed over region outside the warm anomalies (characterized by SSHA < 4 cm, Figure 1a) and experienced a short period of intensity declination (from 110 to 100 kts, Figure 1b). As it returned to the warm anomaly region at 0600 UTC 2 May 2008, its intensity picked up again. Just prior to landfall, Nargis' intensity reached its peak at 115 kts (Figure 1).

[5] From existing literature, positive SSHA feature observed by satellite altimetry indicates warm anomaly relative to the mean climatological condition in the subsurface [Shay et al., 2000; Goni and Trinanes, 2003; Lin et al., 2005, 2008; Pun et al., 2007]. Searching through the Argo

¹Department of Atmospheric Sciences, National Taiwan University, Taipei, Taiwan.

²Jet Propulsion Laboratory, California Institute of Technology, Pasadena, California USA.

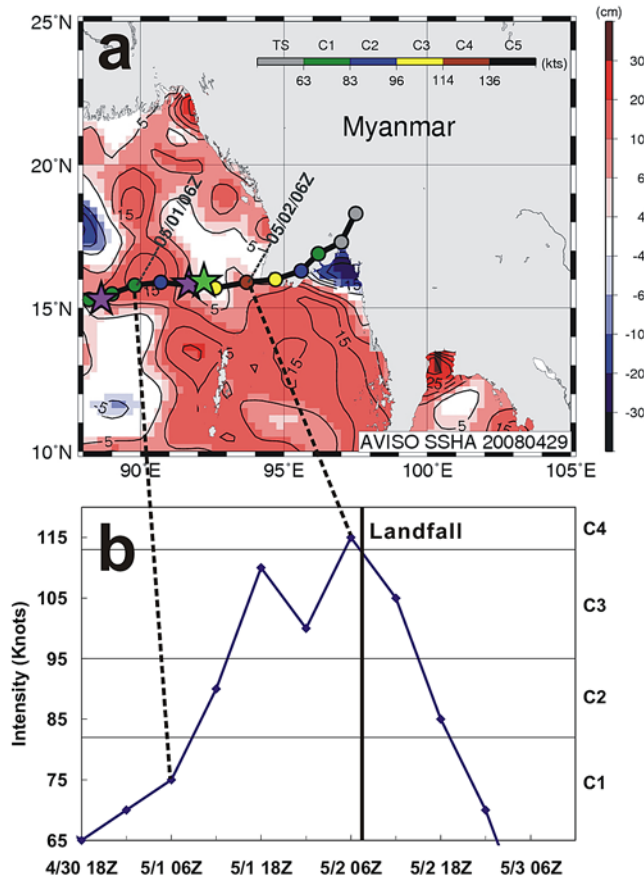


Figure 1. (a) Pre-existing SSHA condition in the Bay of Bengal observed on 29 April 2008 with Nargis' track and intensity (in Saffir-Simpson scale) overlaid. Locations of the searched in situ Argo/GTSPSP profiles are depicted in purple/green stars, respectively. (b) Correspondent time series showing Nargis' rapid intensification, left axis, intensity in kts (1-min maximum sustained wind); right axis, intensity in Saffir-Simpson scale from category-1 to 4.

and the GTSPSP data bases, four in situ depth-temperature profiles in the warm anomaly regions are found. All profiles are on the track (see purple and green stars in Figure 1a) and are acquired about 1 week prior to the RI. These in situ profiles (Table 1) are compared with the climatological profiles along the track (data source: 0.25° spatial resolution data from the NOAA/World Ocean Atlas 2001 [Stephens *et al.*, 2002]) (Figure 2 and Table 2). On locations along the track where no suitable in situ profiles are found, profiles derived from the observed SSHA using the two-layer reduced gravity model [Shay *et al.*, 2000; Goni and Trinanes, 2003; Pun *et al.*, 2007] are used (Table 1). Comparison in sea surface temperature (SST), depth of the 26°C isotherm (i.e., D26, often used to characterize the subsurface warm layer thickness), and the Tropical Cyclone Heat Potential (i.e., the integrated heat content excess per unit area relative to the 26°C isotherm, integrated from D26 to the surface) [Shay *et al.*, 2000; Goni and Trinanes, 2003; Pun *et al.*, 2007; Lin *et al.*, 2008] are made. TCHP is calculated as

$$TCHP = c_p \rho \sum_{i=1}^n \Delta T(x, y, z_i, t) \Delta Z, \quad (1)$$

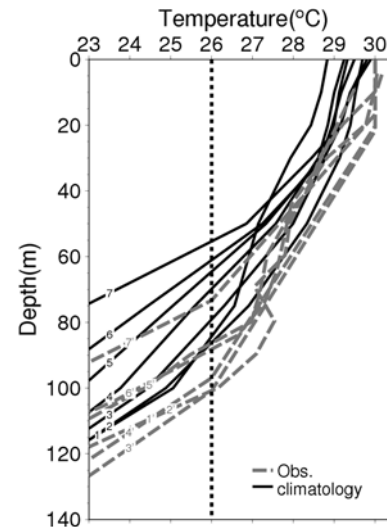


Figure 2. Comparison of the observed pre-storm in situ and altimetry-derived depth-temperature profiles (1'–7') in the warm ocean features (see also Table 1) with the normal climatological profiles (1–7, see also Table 2) along the track.

where c_p is the capacity heat of the seawater at constant pressure taken as $4178 \text{ J kg}^{-1} \text{ °C}^{-1}$, ρ is the average seawater density of the upper ocean taken as 1026 kg m^{-3} , $\Delta T(x, y, z_i, t)$ is the temperature difference between $T(z_i)$ and 26°C at depth z_i , ΔZ is the depth increment taken as 5 m, and n is the total layers from surface to the D26. Thus TCHP is the sum of heat content at each depth increment (ΔZ) through the surface to the D26.

[6] From Tables 1 and 2, and Figures 1 and 2, it can be seen that in the warm anomaly, the SST ranges between 30 and 30.2°C , as compared to the $28.8\text{--}29.9^\circ\text{C}$ climatological SSTs. More evident difference is observed in the subsurface that in the warm features, D26 (and TCHP) can reach as deep as 73–101 m (and $77\text{--}105 \text{ kJcm}^{-2}$) while the climatological D26 (and TCHP) is 55–86 m (and $56\text{--}87 \text{ kJcm}^{-2}$).

3. Numerical Experiments and Air-Sea Flux Estimation

[7] Given the observed pre-existing warm ocean anomaly, what is the impact during the RI process? Using the Price *et al.* [1986] ocean mixed layer model with initial

Table 1. Observed Pre-storm SST, D26, and TCHP in the Warm Ocean Anomaly, Calculated Based on the in Situ and the Altimetry-Derived Profiles^a

Number	Type	Time	Longitude (°E)/ Latitude (°N)	Pre-SST (°C)	Pre-D26 (m)	Pre-TCHP (kJ cm ⁻²)
1'	ARGO	4/22	88.6/15.3	30.0	100.8	95.7
2'	ARGO	4/22	88.6/15.3	30.0	100.8	95.7
3'	Derived	4/29	89.8/15.8	30.0	100.8	105.2
4'	Derived	4/29	90.7/15.9	30.0	96.9	100.6
5'	ARGO	4/23	91.7/15.9	30.2	86.3	83.3
6'	GTSPSP	5/1	92.2/15.9	29.5	88.2	82.0
7'	Derived	4/29	93.7/15.9	30.0	73.3	77.1

^aProfiles 1'–7', as depicted in grey-dashed in Figure 2.

Table 2. Same as Table 1, but for the climatological profiles along the track^a

Number	TrackTime	Longitude (°E)/		Pre-SST	Pre-D26	Pre-TCHP
		Latitude (°N)				
1	4/30 18Z	88.2E	15.3N	28.8	84.3	55.6
2	5/1 00Z	89.0E	15.5N	29.7	86.2	87.3
3	5/1 06Z	89.8E	15.8N	29.3	79.1	72.4
4	5/1 12Z	90.7E	15.9N	29.2	69.8	62.3
5	5/1 18Z	91.7E	15.8N	29.5	64.6	60.9
6	5/2 00Z	92.6E	15.7N	29.8	61.1	62.3
7	5/2 06Z	93.7E	15.9N	29.9	55.4	56.8

^aProfiles 1–7, as depicted in black in Figure 2.

input from profiles in Figure 2 and the drag coefficient from Powell *et al.* [2003], the during-storm UOTS is simulated under progressive periods of intensification. According to the observed translation speed, the simulation is performed and more details of the model set up are given by Lin *et al.* [2008]. For each location on the track, the nearest in situ Argo profile is used as the initial UOTS condition. Two sets of experiments are run, one under the in situ warm ocean anomaly condition (see Table 1, also depicted as the grey-dashed profiles in Figure 2) and the other under the regular climatological condition (see Table 2, also depicted as the black profiles in Figure 2). Figures 3a–3d depict the results during category 1 to 4, respectively. Also in Tables 3 and 4, the pre-storm SST, during-storm SST, and the SST difference for the 2 sets of results are summarised.

[8] In Figure 3, one can see the impact due to the mixing of the cyclone wind when comparing the during-storm UOTS (dashed profiles) with the pre-storm UOTS profiles (solid profiles). Clearly with the mixing from colder waters at deeper layers, the during-storm SST is reduced from the pre-storm values and this storm-induced cooling is more evident under the climatological than the warm-feature condition (Figure 3). For example in Figure 3a, the during-storm SST is reduced to 27.6°C under the climatological condition (black-dashed profile) while the

Table 3. Pre-storm SST, During-Storm SST, and the SST Difference for the 2 Sets of Numerical Experiments During the RI Period Under the Observed Warm Ocean Feature Condition^a

In Situ	4/30	5/1	5/1	5/1	5/1	5/2	5/2
	18Z	00Z	06Z	12Z	18Z	00Z	06Z
pre-SST	30.0	30.0	30.0	30.0	30.2	29.5	30.0
during SST	28.7	28.6	28.8	28.5	27.9	27.8	27.8
Δ SST	-1.3	-1.4	-1.2	-1.5	-2.3	-1.7	-2.2

^aUnit °C.

correspondent during-storm SST under the warm-feature condition is 28.7°C (gray-dashed profile). As expected, with increase in intensity the storm-induced cooling increases. It can be seen that at category-4, the during-storm SST under the climatological condition (black-dashed profile) is reduced to 26.8°C while the correspondent during-storm SST under the warm-feature condition is still relatively high, of value ~27.8°C (gray-dashed profile) (Figure 3d).

[9] How does this difference in the storm-induced cooling impact the available air-sea fluxes for intensification? As shown by Emanuel [1999] and Lin *et al.* [2008], air-sea fluxes are very sensitive to this cooling effect. Using the bulk aerodynamic formulae, the inner-core sensible (Q_S) and latent heat fluxes (Q_L) are calculated [Powell *et al.*, 2003; Black *et al.*, 2007; Lin *et al.*, 2008] as follows:

$$Q_S = C_H W (T_s - T_a) \rho_a C_{pa} \quad (2)$$

and

$$Q_L = C_E W (q_s - q_a) \rho_a L_{va} \quad (3)$$

where C_H and C_E are the sensible and latent heat exchange coefficients, W is the wind speed, T_s and T_a are SST and near surface air temperature, q_s and q_a are

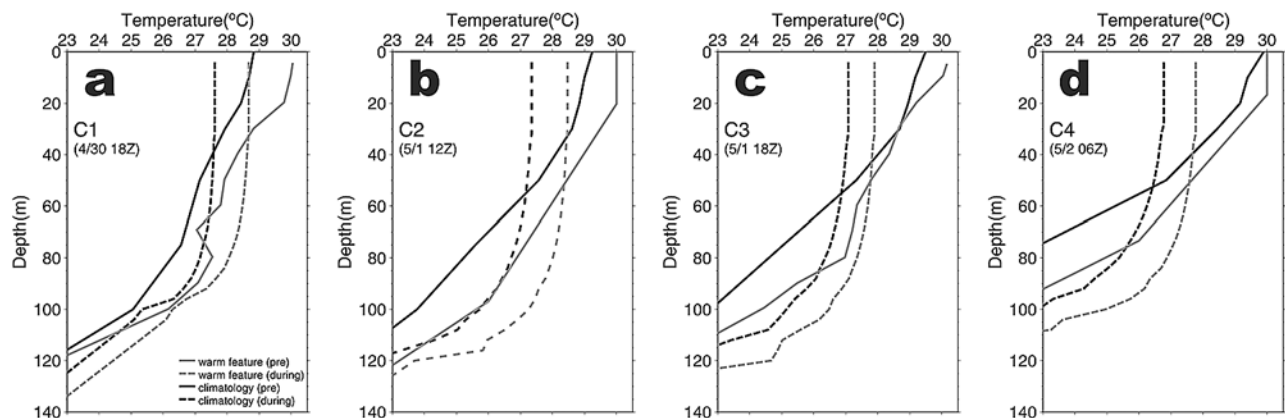


Figure 3. Results from the ocean mixed layer numerical experiments showing the during-storm UOTS from category-1 to 4, respectively. Here gray profiles are for the warm ocean feature condition (solid profile, pre-storm condition; dashed profile, during-storm condition). Black profiles are for the normal climatological condition (solid profile, pre-storm condition; dashed profile, during-storm condition).

Table 4. Pre-storm SST, During-Storm SST, and the SST Difference for the 2 Sets of Numerical Experiments During the RI Period Under the Climatological Condition^a

Climatological Condition	4/30 18Z	5/1 00Z	5/1 06Z	5/1 12Z	5/1 18Z	5/2 00Z	5/2 06Z
pre-SST	28.8	29.7	29.3	29.2	29.5	29.8	29.9
during SST	27.6	28.5	28	27.4	27.1	27.1	26.8
Δ SST	-1.2	-1.2	-1.3	-1.8	-2.4	-2.7	-3.1

^aUnit °C.

surface and air specific humidity, ρ_a , C_{pas} and L_{va} are air density, heat capacity of the air, and latent heat of vaporization. In this study, the exchange coefficients are from *Black et al.* [2007] while the near surface atmospheric data is from the 2.5 resolution NCEP (National Centers for Environmental Prediction) data. Using the same atmospheric data, sensible, latent, and the total enthalpy fluxes (i.e., latent + sensible heat fluxes) are estimated during the RI period for the observed in situ warm-feature condition and the climatological ocean condition (Tables 5 and 6 and Figure 4).

[10] From Tables 5 and 6, it can be seen that latent heat flux is the primary contributor to the total enthalpy during the RI period. Also the available enthalpy provided under the in situ warm-feature scenario is evidently higher than under the climatological scenario, especially towards reaching the peak at category-4 (Figures 1 and 4). It can be found that at 0600 UTC 2 May 2008, the available in situ enthalpy is around 900 W m^{-2} , i.e., a nearly 300% increase in the available enthalpy than under the climatological scenario of around 300 W m^{-2} (Figure 4). This suggests the critical role warm ocean feature plays in providing much more available enthalpy to support the RI. Observing the enthalpy flux time series under the climatological condition (black curve in Figure 4), it can be seen that the available enthalpy flux is predominantly low (typically $\sim 200\text{--}400 \text{ W m}^{-2}$) and at times drops to nearly 100 W m^{-2} (e.g., at 1200 UTC 1 May). This shows that without the presence of the warm feature, it is highly unlikely to support the observed rapid intensification to category 4 within 24 h, given this small amount of enthalpy flux under the climatological condition. Further support on the above can be found in two other similar cases in the western North Pacific (i.e., Typhoon Maemi (2003) and Typhoon Maon (2004)) that encountering warm features are critical in the rapid intensification. As can be seen in the auxiliary material¹, much more available flux can be provided under the warm feature condition, as compared to the climatological condition.

4. Discussion and Conclusion

[11] Finally, it should be clarified that though the focus of this study is on the role of UOTS and the associated air-sea fluxes in Nargis's RI, it does not suggest that other atmospheric factors, such as vertical wind shear or high level

¹Auxiliary materials are available in the HTML. doi:10.1029/2008GL035815.

Table 5. Correspondent Sensible Heat, Latent Heat, and the Total Enthalpy Fluxes for the 2 Sets of Numerical Experiments During the RI Period Under the Observed Warm Ocean Feature Condition^a

	4/30 18Z	5/1 00Z	5/1 06Z	5/1 12Z	5/1 18Z	5/2 00Z	5/2 06Z
SHF	-30	-20	-116	-153	-136	-123	-169
LHF	445	560	587	639	762	773	1036
Total	415	540	471	486	626	650	867

^aSensible + latent heat, total enthalpy. Wm^{-2} , flux under in situ condition.

outflow, is not important [*Frank and Ritchie*, 2001; *Kaplan and DeMaria*, 2003; *DeMaria et al.*, 2005; *Ventham and Wang*, 2007]. For example in this work, vertical wind shear during the RI period is estimated within 500 km radius from the storm centre using the wind field at 200 mb and 850 mb, based on the NCEP data. As depicted in Figure 4, during the RI period the vertical wind shear condition was also favorable, typically around $4\text{--}7 \text{ m s}^{-1}$ between 200 and 850 mb [*Frank and Ritchie*, 2001]. However, since the energy source (i.e., air-sea fluxes) for intensification comes from the ocean, i.e., ocean is a necessary condition in intensification [*Emanuel*, 1999]. Therefore even if the atmospheric conditions are favorable, yet without sufficient flux supply from the ocean, it is not possible for intensification to take place.

[12] In this research, we first present evidences from the in situ UOTS and satellite altimetry SSHA measurements to show that Nargis's RI took place on a pre-existing warm upper ocean anomaly (especially at the subsurface). Next, two sets of ocean mixed layer numerical experiments [*Price et al.*, 1986; *Powell et al.*, 2003] are conducted to compare the during-storm UOTS under the observed warm anomaly condition and under the regular climatological condition. The results show that the presence of warm upper ocean anomaly enables less reduction in storm-induced SST cooling during the intensification process. As a result, much more available air-sea enthalpy fluxes can be supplied to support the rapid intensification, especially towards reaching Nargis' peak at category-4. The estimated enthalpy flux is $\sim 900 \text{ W m}^{-2}$, which is a nearly 300% increase than the nominal supply. In the absence of the warm anomaly, the enthalpy flux is found to be pre-dominantly-low, difficult to support the observed rapid intensification.

[13] This work demonstrates the critical role ocean features played in the RI of the devastating cyclone Nargis (2008). It also highlights the necessity of incorporating such

Table 6. Correspondent Sensible Heat, Latent Heat, and the Total Enthalpy Fluxes for the 2 Sets of Numerical Experiments During the RI Period Under the Climatological Condition^a

	4/30 18Z	5/1 00Z	5/1 06Z	5/1 12Z	5/1 18Z	5/2 00Z	5/2 06Z
SHF	-77	-23	-163	-241	-232	-184	-299
LHF	291	552	428	356	456	580	627
Total	214	528	265	115	223	396	327

^aSensible + latent heat, total enthalpy. Wm^{-2} , flux under climatological condition.

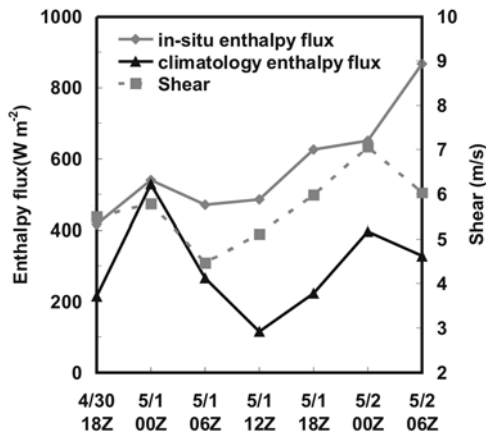


Figure 4. The estimated total enthalpy flux (left axis) and vertical wind shear (right axis) during Nargis' rapid intensification.

ocean subsurface information in future forecast of the Northern Indian Ocean/Bay of Bengal cyclones.

[14] **Acknowledgments.** The authors wish to thank Dong-Ping Wang for providing the mixed layer model, and to Sau Ni Hui for data processing. Thanks also to the NCEP, the AVISO altimetry team, and the Argo float team for data provision. This work is supported by the National Science Council, Taiwan through NSC 97-2111-M-002-014-MY3 and NSC 95-2611-M-002 -024 -MY3. This work is also under Taiwan National Science Council's Integrated Typhoon-Ocean Program (ITOP). The work of W. T. Liu was supported by the National Aeronautics and Space Administration.

References

Ali, M. M., P. S. V. Jagadeesh, and S. Jain (2007), Effects of eddies on Bay of Bengal cyclone intensity, *Eos Trans. AGU*, *88*(8), doi:10.1029/2007EO080001.

Black, P. G., E. A. D'Asaro, W. M. Drennan, J. R. French, P. P. Niller, T. B. Sanford, E. J. Terrill, E. J. Walsh, and J. A. Zhang (2007), Air-sea exchange in hurricanes, *Bull. Am. Meteorol. Soc.*, *88*, 357–374.

DeMaria, M., M. Manelli, L. K. Shay, J. A. Knaff, and J. Kaplan (2005), Further improvements to the Statistical Hurricane Intensity Prediction Scheme (SHIPS), *Weather Forecast.*, *20*, 531–543.

Emanuel, K. A. (1999), Thermodynamic control of hurricane intensity, *Nature*, *401*, 665–669.

Frank, W. M., and E. A. Ritchie (2001), Effects of vertical wind shear on the intensity and structure of numerically simulated hurricanes, *Mon. Weather Rev.*, *129*, 2249–2269.

Goni, G. J., and J. A. Trintanes (2003), Ocean thermal structure monitoring could aid in the intensity forecast of tropical cyclones, *Eos Trans. AGU*, *84*(51), doi:10.1029/2003EO510001.

Gould, J., et al. (2004), Argo profiling floats bring new era of in situ ocean observations, *Eos Trans. AGU*, *85*(19), doi:10.1029/2004EO190002.

Kaplan, J., and M. DeMaria (2003), Large-scale characteristics of rapidly intensifying tropical cyclones in the North Atlantic basin, *Weather Forecast.*, *18*, 1093–1108.

Lin, I.-I., C.-C. Wu, K. A. Emanuel, I.-H. Lee, C.-R. Wu, and I.-F. Pun (2005), The interaction of supertyphoon Maemi (2003) with a warm ocean eddy, *Mon. Weather Rev.*, *133*, 2635–2649.

Lin, I.-I., C.-C. Wu, I.-F. Pun, and D.-S. Ko (2008), Upper ocean thermal structure and the western North Pacific category-5 typhoons. Part I: Ocean features and category-5 typhoon's intensification, *Mon. Weather Rev.*, *136*, 3288–3306.

Powell, M. D., P. J. Vickery, and T. A. Reinhold (2003), Reduced drag coefficient for high wind speeds in tropical cyclones, *Nature*, *422*, 279–283.

Price, J. F., R. A. Weller, and R. Pinkel (1986), Diurnal cycling: Observations and models of the upper ocean response to diurnal heating, cooling, and wind mixing, *J. Geophys. Res.*, *91*, 8411–8427.

Pun, I.-F., I.-I. Lin, C.-R. Wu, D.-S. Ko, and W. T. Liu (2007), Validation and application of altimetry-derived upper ocean thermal structure in the western North Pacific Ocean for typhoon intensity forecast, *IEEE Trans. Geosci. Remote Sens.*, *45*, 1616–1630.

Shay, L. K., G. J. Goni, and P. G. Black (2000), Effects of a warm oceanic feature on Hurricane Opal, *Mon. Weather Rev.*, *128*, 1366–1383.

Stephens, C., J. I. Antonov, T. P. Boyer, M. E. Conkright, R. A. Locarnini, T. D. O'Brien, and H. E. Garcia (2002), *World Ocean Atlas 2001*, vol. 1, *Temperature*, NOAA Atlas NESDIS, vol. 49, NOAA, Silver Spring, Md.

Ventham, J. D., and B. Wang (2007), Large scale flow patterns and their influence on the intensification rates of western North Pacific tropical storms, *Mon. Weather Rev.*, *135*, 1110–1127.

Webster, P. (2008), Myanmar's deadly daffodil, *Nature Geosci.*, *1*, 488–490.

Wu, C.-C., C.-Y. Lee, and I.-I. Lin (2007), The effect of the ocean eddy on tropical cyclone intensity, *J. Atmos. Sci.*, *64*, 3562–3578.

C.-H. Chen, I.-I. Lin (corresponding author), I.-F. Pun, and C.-C. Wu, Department of Atmospheric Sciences, National Taiwan University, Number 1, Section 4, Roosevelt Road, Taipei 106, Taiwan. (iilin@as.ntu.edu.tw)
W. T. Liu, Jet Propulsion Laboratory, California Institute of Technology, 4800 Oak Grove Drive, Pasadena, CA 91011, USA.